Biofuel powered glucose detection in bodily fluids with an n-type conjugated polymer

nature materials

SUPPLEMENTARY INFORMATION

https://doi.org/10.1038/s41563-019-0556-4

In the format provided by the authors and unedited.

Biofuel powered glucose detection in bodily fluids with an n-type conjugated polymer

David Ohayon[1,6], Georgios Nikiforidis[1,6], Achilleas Savva[1], Andrea Giugni[2], Shofarul Wustoni[1], Tamilarasan Palanisamy[2,5], Xingxing Chen[2], Iuliana Petruta Maria[3], Enzo Di Fabrizio[2], Pedro M. F. J. Costa[2], Iain McCulloch[2,3,4] and Sahika Inal[1]*

[1]Biological and Environmental Science and Engineering Division, King Abdullah University of Science and Technology (KAUST), Thuwal, Saudi Arabia. [2]Physical Science and Engineering Division, KAUST, Thuwal, Saudi Arabia. [3]Department of Chemistry and Centre for Plastic Electronics, Imperial College London, London, UK. [4]KAUST Solar Center, KAUST, Thuwal, Saudi Arabia. [5]Present address: Electrodics and Electrocatalysis Division (EEC), CSIR-Central Electrochemical Research Institute (CSIR-CECRI), Karaikudi, India. [6]These authors contributed equally: David Ohayon, Georgios Nikiforidis.
*e-mail: sahika.inal@kaust.edu.sa

Supporting information

Biofuel Powered Glucose Detection in Bodily Fluids with an n-type Conjugated Polymer

David Ohayon,[1] Georgios Nikiforidis,[1] Achilleas Savva,[1] Andrea Giugni,[2] Shofarul Wustoni,[1] Tamilarasan Palanisamy,[2] Xingxing Chen,[2] Iuliana Petruta Maria,[3] Enzo Di Fabrizio,[2] Pedro M. F. J. Costa,[2] Iain McCulloch,[2,3] Sahika Inal[1*]

[1] Biological and Environmental Science and Engineering Division, King Abdullah University of Science and Technology (KAUST), Thuwal 23955-6900, Saudi Arabia.
[2] Physical Science and Engineering Division, KAUST, Thuwal 23955-6900, Saudi Arabia.
[3] Department of Chemistry and Centre for Plastic Electronics, Imperial College London, London SW7 2AZ, United Kingdom.

*Corresponding author: sahika.inal@kaust.edu.sa

Table S1. Comparison of K_m^{app} values obtained in this study with those of other reported for high-performance systems.

Materials	GOx immobilization	K_m^{app} / mM	Ref.
PVA-g-P(4-VP) films	Physical entrapment	19	[1]
Nafion film	Covalent attachment with GA, BSA and Nafion	14.91	[2]
Chitosan matrix	Covalent attachment with GA in a 5% (v/v) glycerol solution	14.2	[3]
NiO modified glassy carbon electrodes	Co-deposition with NiO nanoparticles at 0.8 V for 15 min in buffer solution	2.7	[4]
Gold nanoparticles	Thiol-Cystamine modification of Au with IO_4^- oxidized GOx	4.3	[5]
Carbon/polymer based materials	Layer by layer deposition with final covalent attachment with GA	0.3	[6]
CNT/PEI composites	Electrostatic attraction	4.3	[7]
CNT-chitosan	Physical entrapment	8.2	[8]
Carbon nanodots	Physical adsorption (Nafion coating on top)	0.85	[9]
PEDOT nanofibers	Covalent attachment with GA	0.91-4.28	[10]
P-90	Physical adsorption	1.73	This work

PVA-g-P(4-VP): poly(vinyl alcohol) grafting 4-vinylpyridine; CNT/PEI: carbon nanotubes/ Polyethyleneimine; GA: glutaraldehyde; BSA: bovine serum albumin

The Michaelis-Menten constant (K_m^{app}) represents the glucose concentration for which the enzymatic reaction runs at half of its maximum velocity. The apparent constant is determined from the electrochemical equivalent of the Lineweaver-Burk equation:[11]

$$\frac{1}{I_D} = \frac{K_M^{app}}{I_{max}} * \frac{1}{C} + \frac{1}{I_{max}} \qquad (1)$$

where I_D and I_{max} are the current output at a given glucose concentration, and the maximum current measured when the sensor current no longer increases with glucose addition, and C is the glucose concentration. From the linear relationship between the inverse of the steady-state current and the analyte concentration extracted from **Fig. 1B**, we calculate the K_m^{app}.

Table S2. Comparison of k_{ET} values found in this work with reported values of other EFCs.

Template for GOx	k_{ET}/ s^{-1}	Ref.
CNT/GA/POx	0.046	[12]
MCF(TOA-Au NP)/GOx	6.0	[13]
CNT/TiO_2/GOx	3.96	[14]
PEI/CNT/GA/GOx	8.6	[6]
CP/GOx	12.1	[15]
Graphene/SWCNT cogel/GOx	0.23	[16]
CNT/PEI/PCA/GOx	11.5	[17]
CNC/CS/GC/GOx	6.0	[18]
CNT-modified/GC/GOx	1.0	[19]
Au/P-90/GOx	8.1	This work

POx: Pyranose oxidase; PEI: poly(ethylenimine); MCF: Metallic cotton fiber; CP: Carbon paper; PCA: pyrenecarboxaldehyde; CNC: Carbon nanochips; CS: Chitosan; GC: Glassy carbon electrode; TOA-Au NP: tetraoctylammonium bromide-stabilized Au nanoparticle

The k_{ET} of the P-90/GOx system is *ca.* 8.11 s^{-1} at 400 $mV.s^{-1}$. These values are as favorable as the ones reported in the literature for analogous systems and attest to the seamless nature of the polymer/enzyme interface and the ability of the polymer to provide a suitable environment for GOx to transfer electrons.

Table S3. Comparison of the performance of previously reported glucose EFCs with this work.

Anode (Electrode support)	Cathode (Electrode Support)	Solution	OCV (V)	MPD ($\mu W.cm^{-2}$)	Stability	Ref.
CDH (spectrographic graphite)	Laccase (spectrographic graphite)	Citrate buffer pH 4.5, 5 mM glucose	0.73	>5	25 h	[20]
CDH (graphite)	BOx (graphite)	PBS buffer, pH 7.4, 5 mM glucose	0.62	3	>6 h	[21]
		Serum	0.58	4	<2 h	
GOx (Au/Nafion-PVP nanowire/CNT)	Laccase (Au/Nafion-PVP nanowire)	PBS buffer, pH 7.4, 5 mM glucose	0.23	31	-	[22]
GOx (CNT disk)	Laccase (CNT disk)	PBS buffer, pH 7.4, 5 mM glucose	0.95	1300	2.7 h	[23]
CDH (Au nanoparticles)	BOx (Au nanoparticles)	PBS buffer, pH 7.4, 5 mM glucose	0.66	3.2	30 h	[24]
CDH (Au NPs/Au μ–wire)	BOx (Au NPs/Au μ–wire)	tear	0.57	3.5	>10 h	[25]
GOx (Carbon nanodots)	BOx (Carbon nanodots)	PBS buffer, pH 7.4, 4 mM glucose	0.93	40.8	-	[9]
GOx (PEI/CNTs)	Laccase (PEI/CNTs)	0.01 M PBS buffer, pH 3, 40 mM glucose,100 $cc.min^{-1}$ O_2	-	102	77% of MPD after 4 weeks	[6]
GOx (Glassy carbon/PANI-CNT)	Laccase (Glassy carbon/PANI-CNT)	PBS buffer, pH 7.2, glucose concentration not mentioned	0.78	1120	83% of current density after 15 days	[26]
GOx (Glassy carbon/Carbon nanochips)	(Pt)	PBS buffer, pH 7.2, 10 mM glucose	0.59	55	-	[18]
GOx (PEI/CNTs)	Laccase (PEI/CNTs)	0.2 mM UA, 0.9 mM AA, 140 mM NaCl, 5 mM glucose	-	180	89% of the MPD after 16 days	[7]
GOx/Fc (graphene coated carbon fiber cloth)	BOx (graphene coated carbon fiber cloth)	PBS buffer, pH 7.4, 200 mM glucose	0.43	34.3	24 h	[27]

FAD/GDH /NQ-LPEI (Toray carbon paper)	BOx/ AnMWCNT (Toray carbon paper)	PBS buffer, pH 7.4, 50 mM glucose / pH 5.6	0.78	360	>1.5 h	[28]
GOx (P-90)	p(EDOT-co-EDOTOH)	PBS buffer, pH 7.4, 10 mM glucose	with membrane: 0.31	with membrane: 2.7	with membrane: 40% of power density recorded at 1 V / 30% OCV retention after 50 days	This work
			membrane-free: 0.185	membrane-free: 0.4	membrane-free: 40% of power density recorded at 1 V / 75% OCV retention after 30 days.	

CDH: cellobiose dehydrogenase; BOx: bilirubin oxidase; PVP: poly(vinyl pyrrolidone); PEI: Polyethylenimine; Fc: Ferrocene; GDH: Glucose dehydrogenase; NQ-LPEI: napthoquinone-4-glycidyl-modified linear poly(ethylenimine); AnMWCNT: anthracene multi walled carbon nanotubes; - : not provided

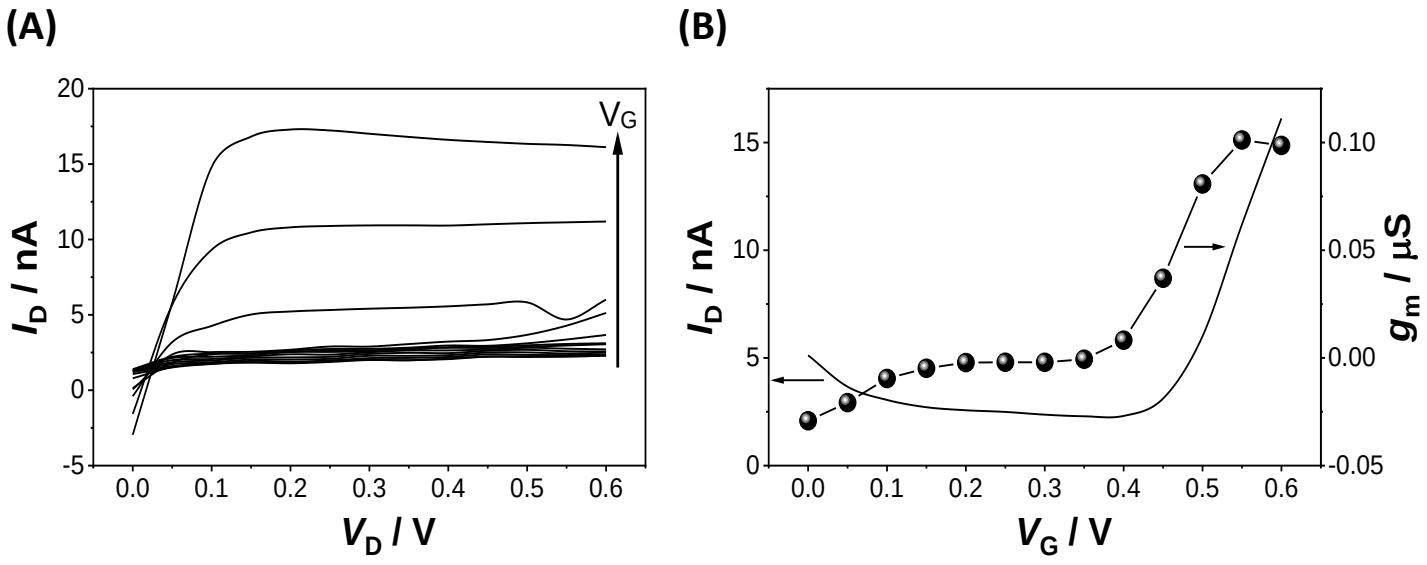

Figure S1. N-type OECT characteristics. **(A)** Device output characteristics recorded in PBS. The drain current (I_D) is measured as a function of drain voltage (V_D) for a given gate voltage (V_G). The drain and gate potentials are swept between 0 and 0.6 V with a step of 0.05 V. **(B)** Transfer characteristics of the device as well as the transconductance (g_m) *vs.* V_G. The channel dimensions are 10 µm in length and 100 µm in width, while the gate electrode has an active area of 500 × 500 µm^2. The gate electrode is a planar Au pattern coated with P-90.

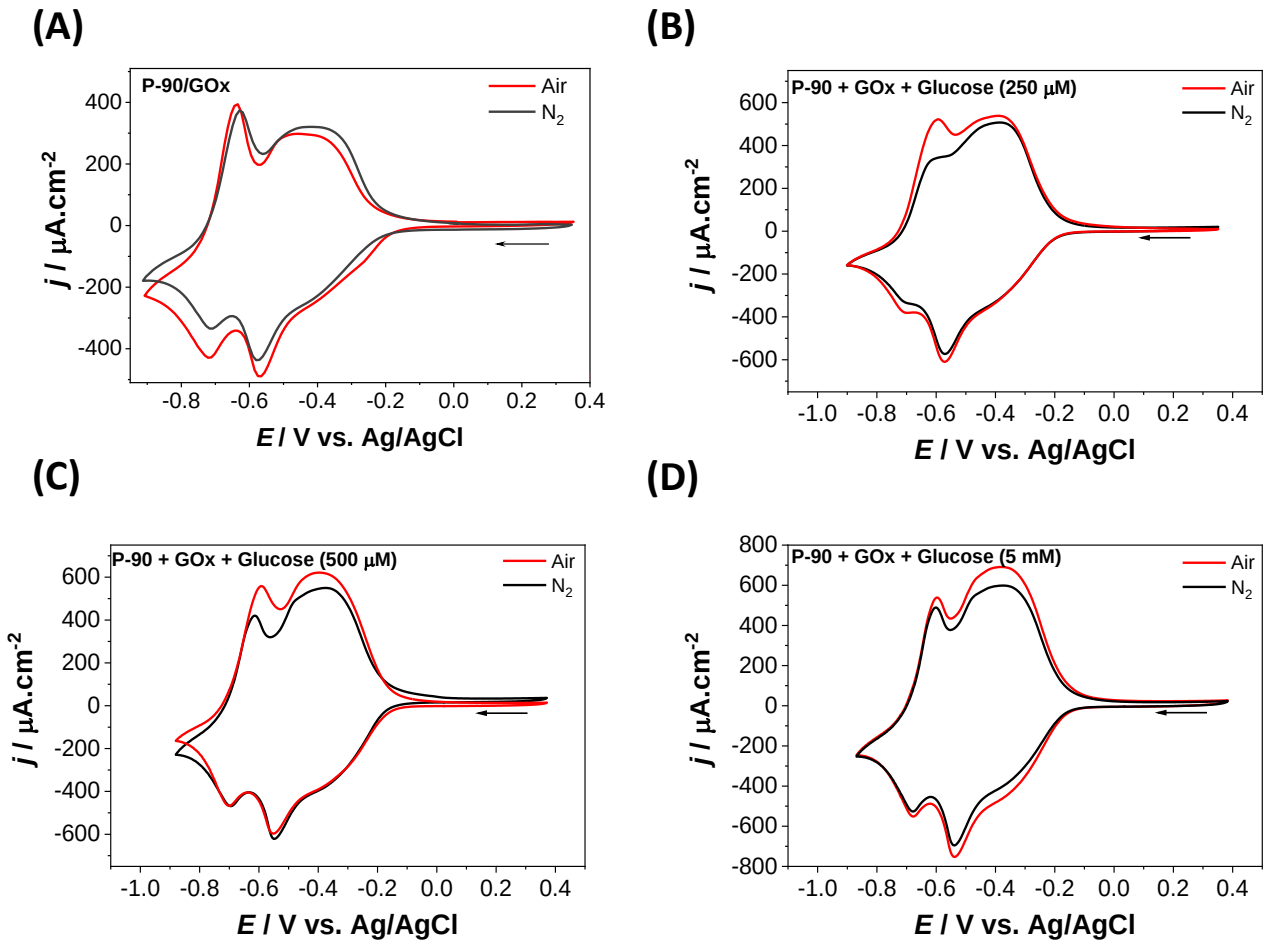

Figure S2. Cyclic voltammogram of P-90/GOx system recorded in PBS in air (red) and inert atmosphere (black) in the absence **(A)** and in the presence **(B) (C) (D)** of glucose. Scan rate is 40 $mV.s^{-1}$. Arrows indicate the scan direction.

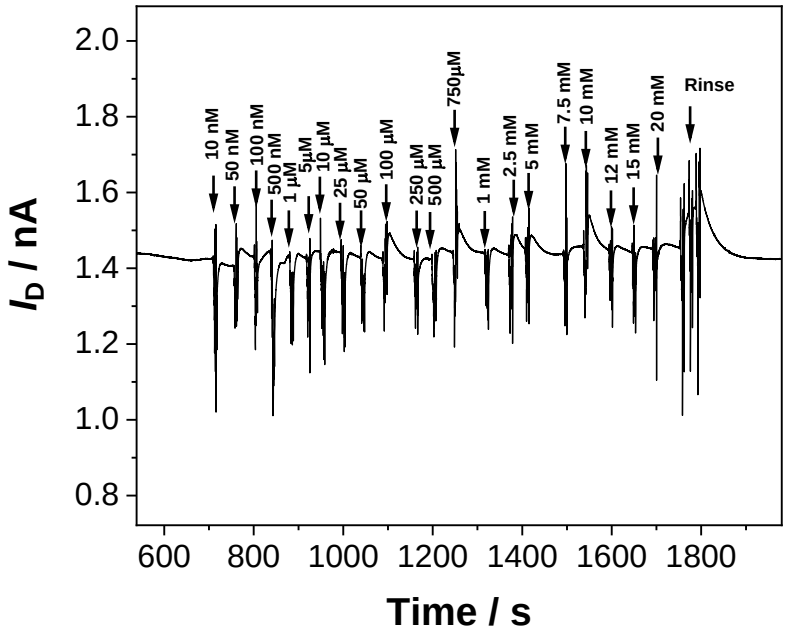

Figure S3. Real-time response of the OECT (source-drain current, I_D, as a function of time) as successive amounts of glucose were added to PBS. The gate and drain potentials applied were 0.5 V and kept constant. For this experiment, the P-90 film at the channel and the gate was functionalized with denatured GOx.

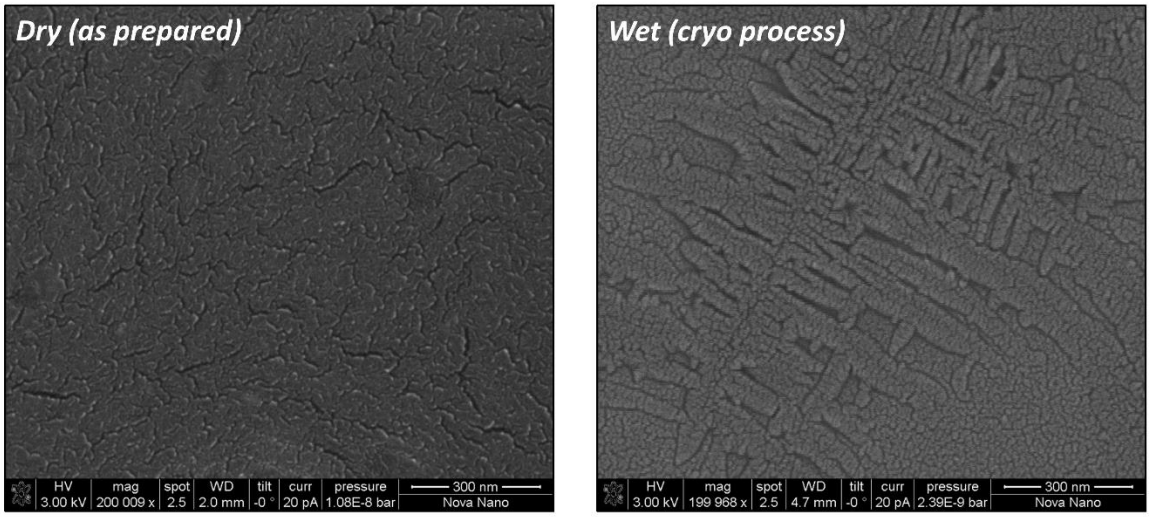

Figure S4. SEM image of P-90 film in dry (left) and wet (right) conditions.

When the P-90 film is incubated with GOx, the enzyme adsorbs on P-90 without prior surface treatment because of the glycol rich regions of the surface. We observed a similar phenomenon when investigating the interactions of synthetic zwitterionic lipid vesicles with a library of P-90 analogs including the P-0.[29] Liposomes favored the ethylene glycol-rich regions on a given film surface and did not adhere on the P-0 film which has limited wettability.

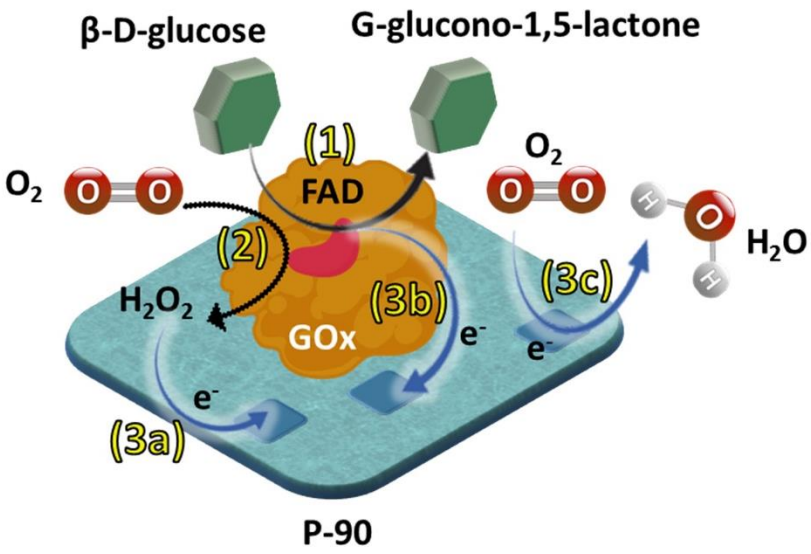

(1) GOx $(FAD)^{P\text{-}90}$ + β-D-glucose → GOx $(FADH_2)^{P\text{-}90}$ + G-glucono-1,5-lactone

(2) GOx $(FADH_2)^{P\text{-}90}$ + O_2 → GOx $(FAD)^{P\text{-}90}$ + H_2O_2

(3a) $H_2O_2 + 2H^+ + 2e^-$(P-90) → $2\ H_2O$

(3b) GOx $(FADH_2)^{P\text{-}90}$ → GOx $(FAD)^{P\text{-}90} + 2H^+ + 2e^-$

(3c) $O_2 + 2H^+ + 2e^-$(P-90) → $H_2O_2 + 2H^+ + 2e^-$(P-90) → $2\ H_2O$

Figure S5. Schematic showing possible mechanisms that take place upon oxidation of glucose by GOx at the P-90 interface.

During the enzymatic reaction, the redox center of the enzyme (flavin adenine dinucleotide, FAD) reacts with glucose and is reduced to $FADH_2$, while glucose gets oxidized to gluconolactone via a two electron transfer process.[30] The enzyme is re-oxidized through electron transfer to an electron acceptor. In the absence of synthetic electron mediators, this electron acceptor is O_2, while the catalytically detectable by-product of the reaction is H_2O_2.[30-31] P-90 competes with O_2 to harvest the electrons.

In situ Raman Spectroscopy - further discussion

In the P-90 spectrum, the region between 1100 and 1800 cm^{-1} refers to the resonant region of carbon bonds in the molecule, that is, the backbone, while the low energy region (<1100 cm^{-1}) are associated with the side-chains. We attribute the three main peaks in the former region to the collective C=C−C bonds stretching/shrinking confined on the T2 unit (1457 cm^{-1}), the NDI unit (1407 cm^{-1}), and to the delocalized vibrations of the NDI-T2 monomer (1431 cm^{-1}) (Fig. 2C, inset).[32] These modes, called Я-modes,[33] represent the vibrational trajectory that best favors the oscillations of the C=C−C bonds-length alternation, and as such, they are the most sensitive to the π-electron perturbations. In other words, vibrations have only a partial Я character, so it can be assumed that the intensity of such modes is proportional to their Я fraction, which is responsible also for its dispersion character. We attribute the peaks at 1709 cm^{-1}, 1612 cm^{-1}, and 1574 cm^{-1} to symmetric stretching vibrations of C=O, C=C, and C=N of the NDI unit, respectively (**Extended Data Fig. 3D inset)**. Finally, we relate other minor vibrations at 1118, 1232, and 1301 cm^{-1} to CH and CH2 modes.

Upon adsorption of the enzyme on the P-90 film, we observe a minor increase in the intensity of the C=O, C=C, and C=N peaks of NDI unit while the Я-modes remain unaffected (**Extended Data Fig. 3D**). Note that we do not observe any new peaks here, presumed to be due to the non-resonant (limited) Raman efficiency of the protein. Raman signals are sensitive to changes in the polarizability of the molecule. The polarizability change induced by the enzyme is lower than that induced by electrochemical doping, suggesting that there is a partial overlap of the electron clouds of the two molecules due to their proximity, affecting the electronic charge distribution of the backbone.

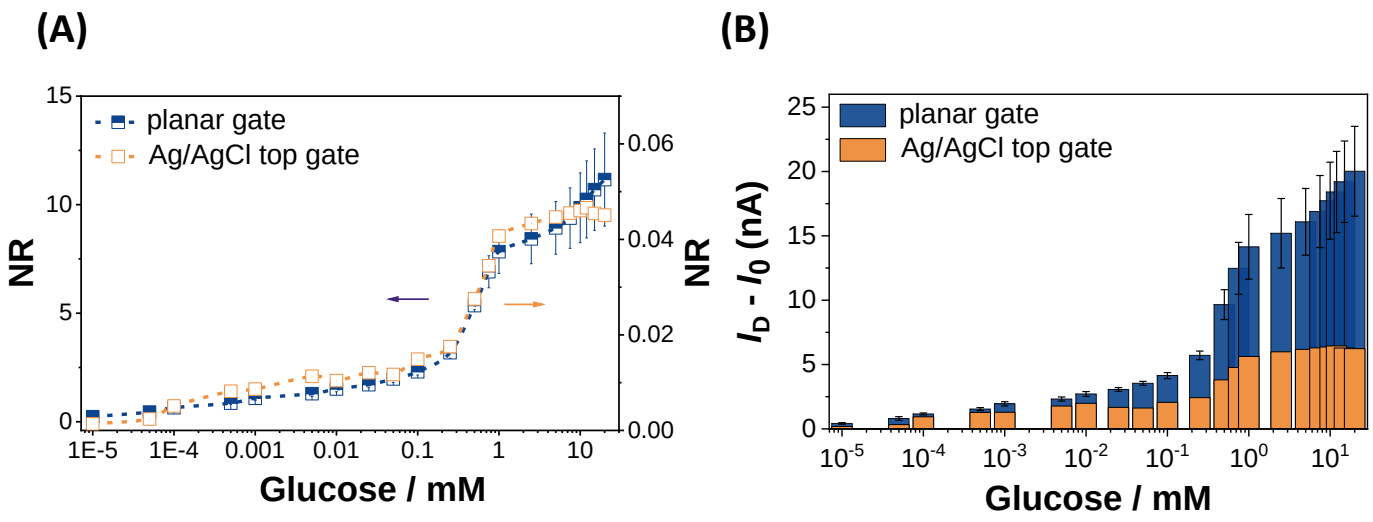

Figure S6. Biosensor performance when gated with P-90 or Ag/AgCl gate **(A)** Normalized response (NR) of the OECT biosensor to glucose using P-90 coated planar gate (left axis) and Ag/AgCl top gate (right axis). **(B)** Relative change in the drain current ($I_D - I_0$) to glucose. The devices were operated at constant V_G = 0.5 V and V_D = 0.6 V using P-90 coated planar gate and Ag/AgCl top gate. The employed log scale improves visualization of the response to low analyte concentrations.

As the reaction takes place both at the channel, and the gate, the sensitivity to low glucose concentrations is enhanced. To demonstrate that the reaction can take place only at the channel, we gate the channel with an external Ag/AgCl pellet immersed in the solution. While the sensor shows comparable sensitivity to glucose, the change in the drain current is much smaller (**Fig. S6**).With the n-type polymer, we can use the channel as the functional layer, and the gate can practically be any metal physically separated from the active area. We envisage this property to be beneficial when designing implantable metabolite sensors. On the other hand, using an integrated, lateral P-90 gate as the sensing layer leads to larger absolute changes in the drain current with glucose, and enhances the sensitivity to high glucose concentrations (because of a larger bio-electronic interface). Although it is challenging to decouple the contribution of each interface on the sensing performance (gate/enzyme, channel/enzyme), we highlight that the device sensitivity can be tuned for detection at a particular concentration range simply by changing the operating conditions, alleviating the need to change its design. These features are inherent to the n-type

polymer and accumulation mode OECT operation with high transconductance, not feasible with the typical p-type and/or depletion mode devices.[34-35]

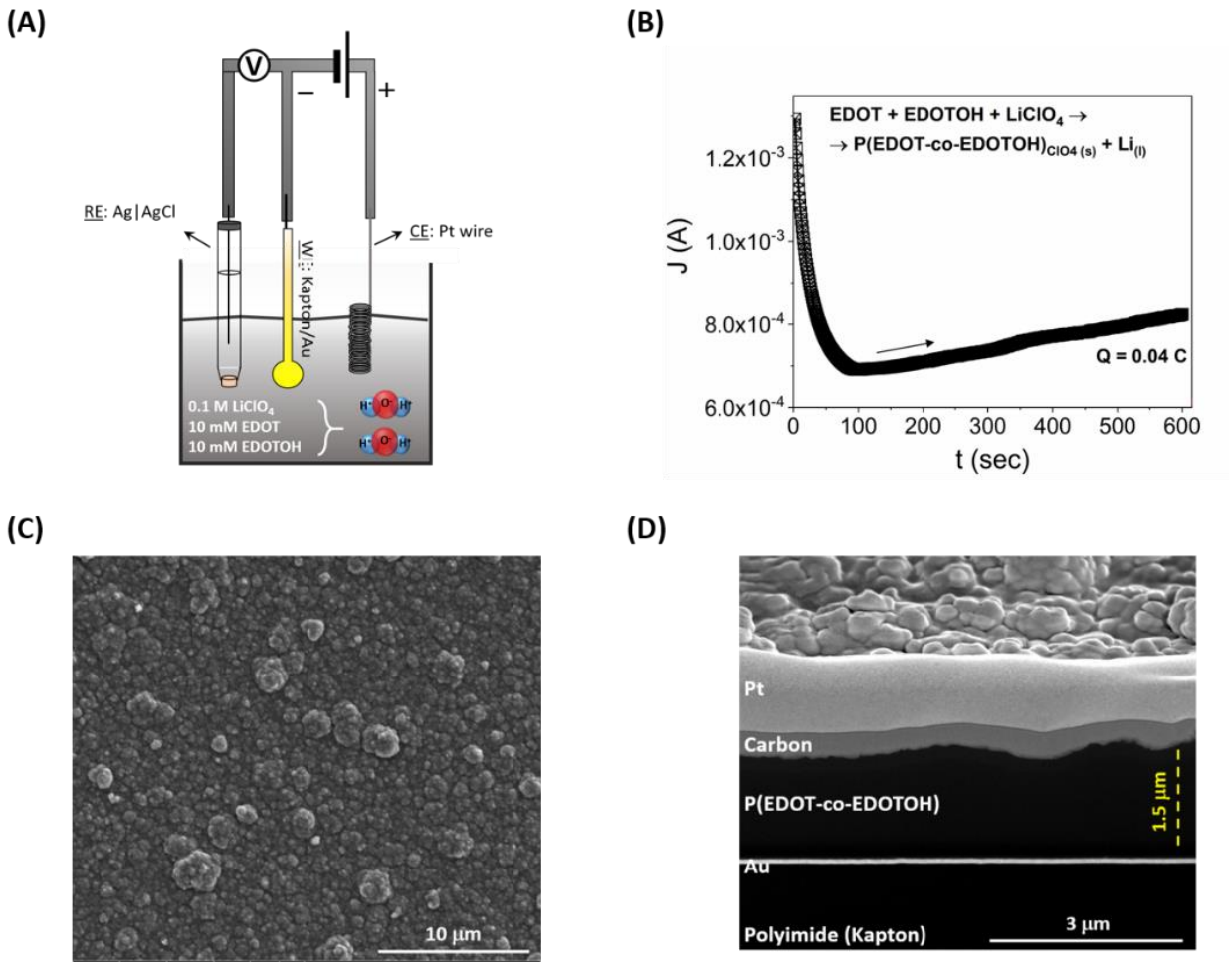

Figure S7. Electropolymerization of the EFC cathode. **(A)** Schematic showing the experimental set-up for the electrodeposition of p(EDOT-co-EDOTOH) **(B)** Chronoamperometry under 1 V *vs.* Ag/AgCl at 25°C. **(C)** SEM image of the cathode film exhibiting a structured surface populated with small granules. **(D)** Cross-sectional FIB-SEM image of p(EDOT-co-EDOTOH) film, having a thickness of 1.5 µm.

ORR of the cathode - further discussion on Extended Data Fig. 4

The number of electrons involved in the ORR is extracted from the slope of each curve (Reciprocal of current density of p(EDOT-co-EDOTOH) vs the rotation speed) and plotted for a specific potential of the voltammogram according to the following equation:[36]

$$n = \frac{B}{0.62FC_oD_o^{2/3}\nu^{-1/6}}$$

where n is the number of electrons, B is the slope of each curve, F is the Faraday constant (96485 $C.mol^{-1}$), C_o is the saturated concentration of O_2 in the electrolyte (1.2×10^6 $mol.cm^{-3}$), D_o is the O_2 diffusion coefficient (1.9×10^{-5} $cm^2.s^{-1}$)[36] and ν is the kinematic viscosity of the electrolyte (PBS).

According to **Extended Data Fig. 4C**, at low negative potentials (≤-0.375 V) the system follows a 4 e^- direct reduction of oxygen to water. As the potential increases in magnitude, the number of electrons involved in the ORR decreases to 2, indicative of an indirect ORR pathway proceeding with H_2O_2 formation.

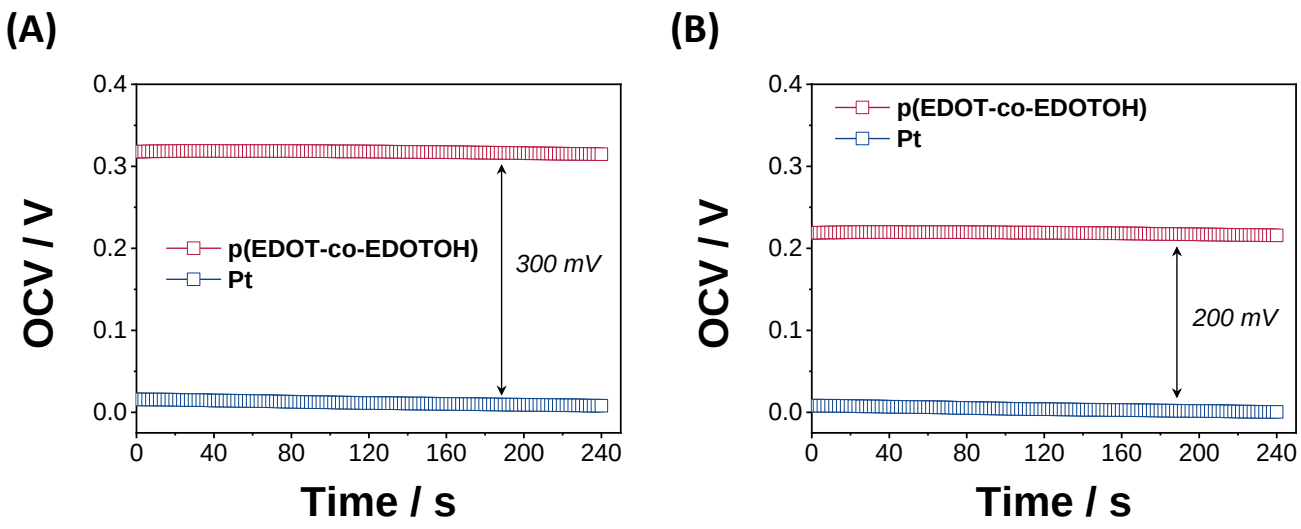

Figure S8. Open circuit voltage (OCV) of P-90/GOx based EFCs having different cathodes, Pt or p(EDOT-co-EDOTOH). The EFCs in (**A**) have a Nafion membrane while those in (**B**) do not. Measurements are performed in PBS containing 1 mM of glucose. Upon enzymatic reaction with 1 mM of glucose, we draw 0.2 V from the membrane-free EFC under open circuit conditions, somehat lower than the theoretical OCV (**Extended Data Figure 5**). We attribute this discrepancy to the overpotential losses originating from the semiconducting nature of the anode.

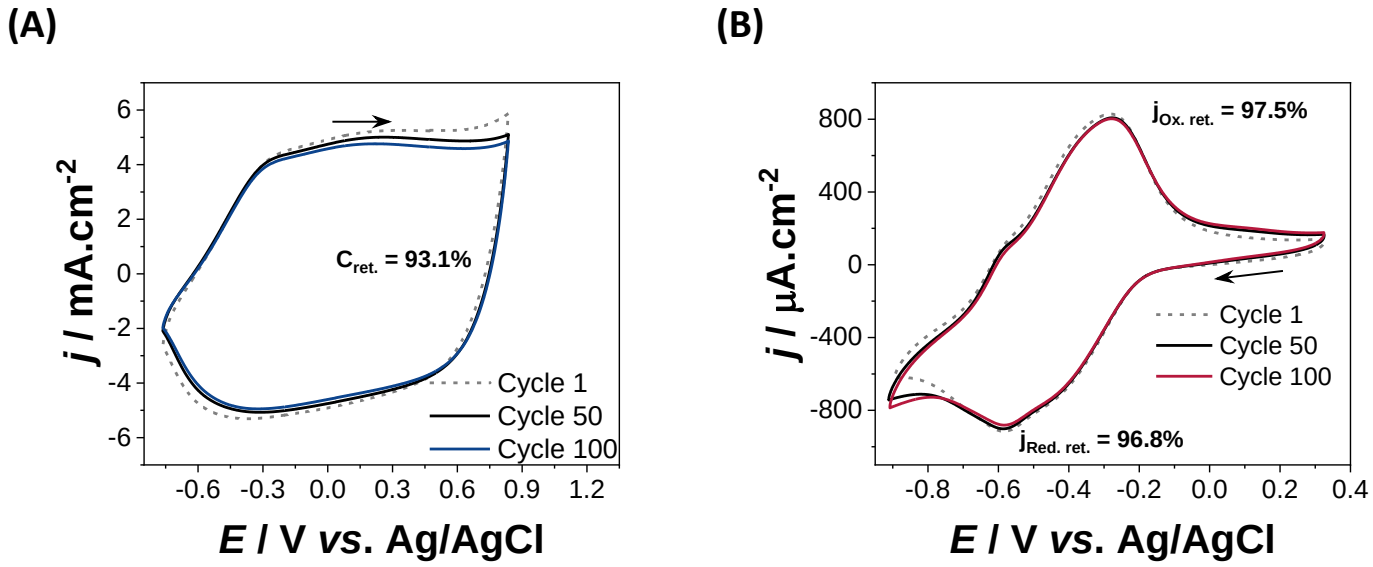

Figure S9. Stability of EFC electrodes. The CV curves of **(A)** the cathode p(EDOT-co-EDOTOH) and **(B)** the bioanode P-90/GOx are measured in PBS over 100 cycles. Scan rate is 100 $mV.s^{-1}$. Arrows indicate the scan direction. C_{ret}: capacitance retention, $J_{Ox.ret}$: oxidation current retention, and $J_{Red.ret}$: reduction current retention.

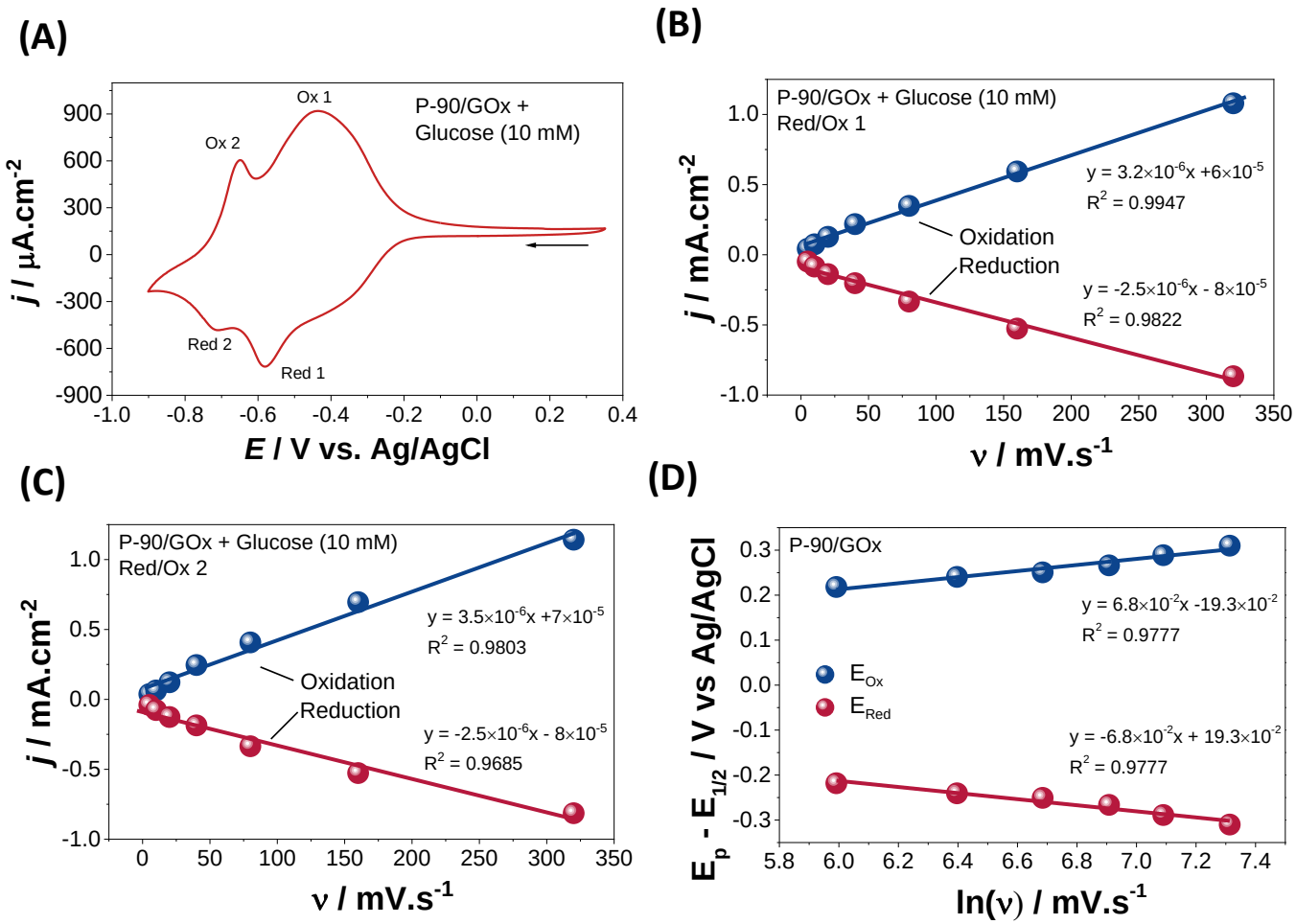

Figure S10. Electrochemical characterization of the bioanode performed in PBS containing 10 mM of glucose. In **(B)** and **(C)**, the current density is plotted as a function of the scan rate for the two distinct redox couples marked in the CV curve shown in **(A)**. The linear relationship between current density and scan rate corroborates a surface-controlled process. **(D)** Laviron plots for the oxidation and reduction reactions. The peak potentials are plotted against the logarithm of the scan rate. At high scan rates, the linear relationship between ΔE_{pp} and ln(ν) yields the electron transfer coefficient (α).

According to the model, the anodic and cathodic peak-to-peak separation ($\Delta E_{pp} = E_p - E_{1/2}$) at high scan rates (ν = 100 mVs^{-1}) should be linear to the logarithm of the scan rate:[37]

$$E_{PC} = E^{\circ} - \frac{R*T}{\alpha*n*F}\ln(\frac{\alpha*n*F}{R*T*k_{ET}} * \nu)$$

$$E_{PA} = E^{\circ} + \frac{R*T}{(1-\alpha)*n*F}\ln(\frac{(1-\alpha)*n*F}{R*T*k_{ET}} * \nu)$$

where E^{o} is the formal potential ($E_{Ox} - E_{Red}$), n is the number of transferred electrons, α is the electron transfer coefficient (related to the symmetry of the redox reaction), and v is the scan rate. From the slope of the curves, the α values were assigned equal to 0.5, suggesting a symmetrical redox process, while n was *ca.* 1.72, close to the two electron reaction involved in the glucose oxidation. k_{ET} can then be extracted as:

$$\log(k_{ET}) = \alpha * \log(1-\alpha) + (1-\alpha) * \log(\alpha) - \log\left(\frac{R*T}{*n*F*\nu}\right) - \alpha(1-\alpha) * \frac{\Delta E_P * n * F}{2.3 * R * T}$$

The k_{ET} of the P-90/GOx system is *ca.* 8.11 s^{-1} at 400 $mV.s^{-1}$.

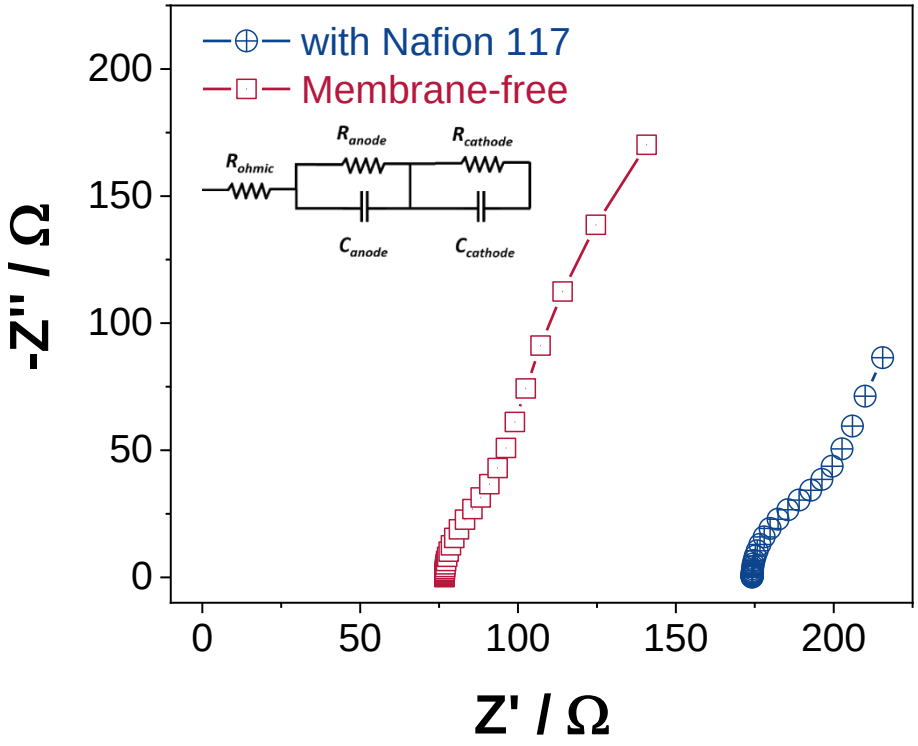

Figure S11. Nyquist plots of the EFC with and without Nafion membrane. Inset shows the equivalent circuit of the EFC. The circuit consists of three parts. The first part is the ohmic component which accounts for the electrolyte resistance between the anode and cathode. The other two parts model the anode (P-90/GOx) and the cathode (p(EDOT-co-EDOTOH)) compartments of the cell. Both anode and cathode polymer films include a capacitor that represents the double layer charging at the surface of the polymer and a resistor that depicts the interfacial resistance between electrode and electrolyte.[38-39] The overall resistance of the cell is the sum of these three parts ($R_{\text{membrane-free}}$ = 600 *vs.* $R_{\text{Nafion 117}}$ = 787 Ω).

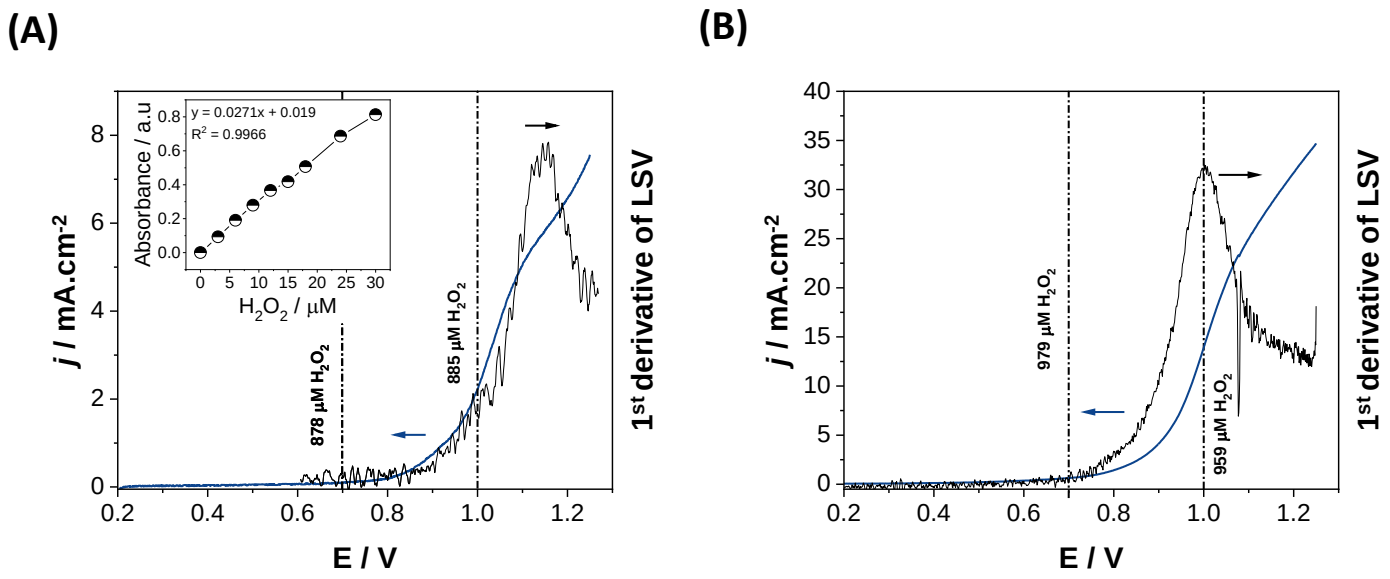

Figure S12. Extended positive linear sweep voltammogram of the cell **(A)** with and **(B)** without a Nafion membrane in the presence of 1 mM of glucose. The current was collected at a scan rate of 5 $mV.s^{-1}$. Through the first derivative of the voltammogram, the inflection point is defined, giving in turn the voltage at which the rate of increase of the redox reactions in the cell reaches a maximum. The current value at the inflection point is used to calculate the power output of the cell for the stability studies. The amount of H_2O_2 in the cell at 0.3, 0.7 and 1 V was determined using a colorimetric assay as described in the Experimental Section.[38,40] Inset of (**A**) shows the H_2O_2 calibration curve.

Note that unless it is operated at high positive voltages, the cell does not produce H_2O_2: the oxidation of glucose at the anode is not O_2-mediated (**Fig. S2**) while the ORR of the cathode proceeds through the pathway that leads to water (**Extended Data Fig. 4**).

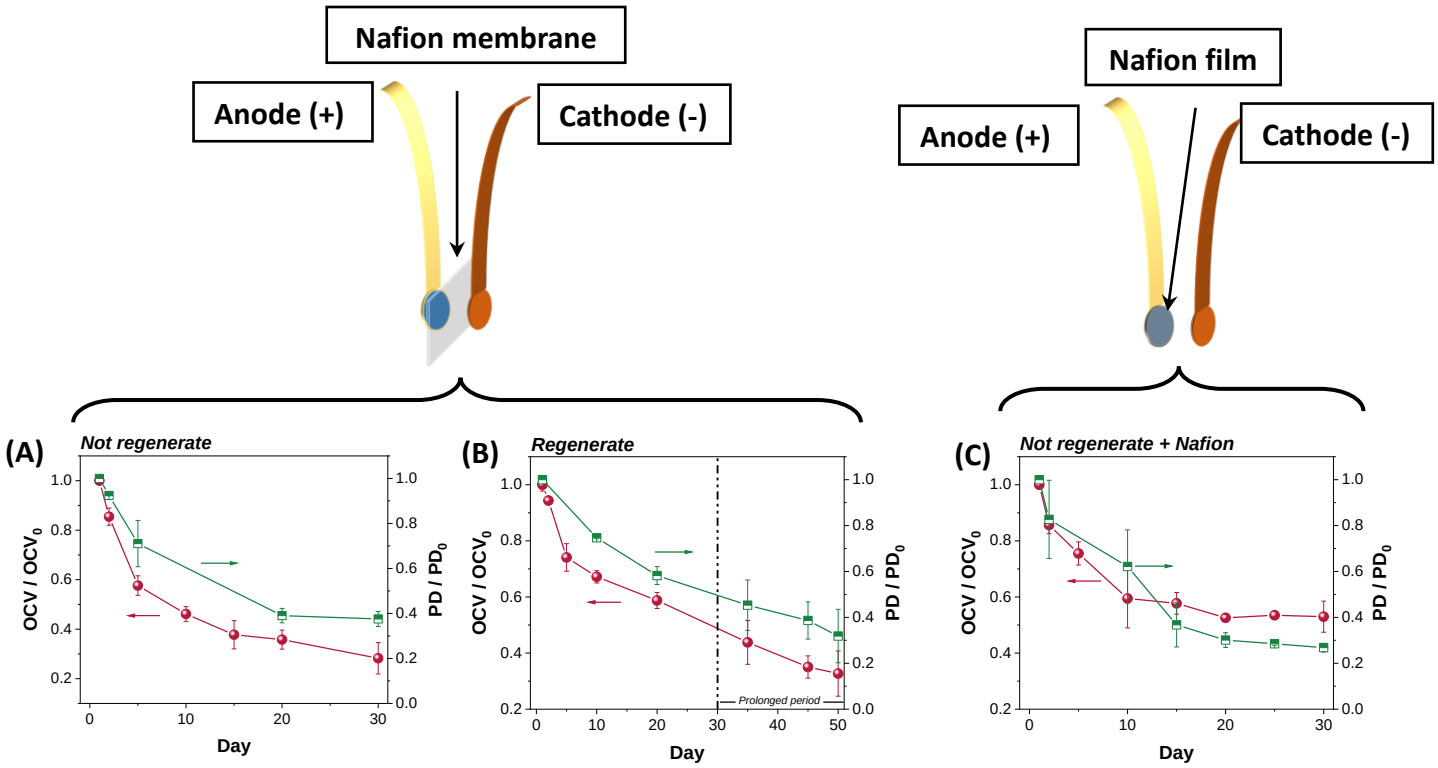

Figure S13. Long term stability of the EFC. Relative voltage (OCV/OCV_0) measured at open circuit conditions and relative power density (PD/DP_0) of the EFC fueled by 1 mM of glucose in PBS. The PD values are determined at an anodic bias (e.g. 1 V, see Figure S19). (**A**) The enzyme is adsorbed on the anode at day 0 and kept as is until day 30, (**B**) the enzyme is replenished before each measurement and measurements continued for 50 days. The anode and cathode are separated with a Nafion membrane (123 μm) as depicted in the top schematic. (**C**) The enzyme is adsorbed on the anode at day 0 and kept as is until day 30. A Nafion film was cast on top of GOx functionalized anode as depicted in the top schematic and used as the encapsulation layer. The error bars show the standard deviation of the mean value of OCV and PD values for four independent measurements.

When the enzyme is not replenished (**Figure S13A**), the OCV drops to 20% of its original value after 30 days, while the EFC retains 40% of its initial PD. When we reload the GOx on the P-90 between measurements (**Figure S13B**), the EFC withholds 60% and 45% of its OCV and PD, respectively. In this configuration, the PD is stable for an additional period of 20 days (50 days in total). The drop in the retention of PD and OCV suggests that i) the enzyme suffers from

denaturation, ii) the polymers undergo some degree of change in their electrochemical state, mostly attributed to the instability of the cathode (p(EDOT-co-EDOTOH) as the P-90 did not show any sign of degradation in OECTs for over 6 months. Diligent choice of encapsulation materials and optimization of the cathode are effective strategies to improve the overall stability of the EFC. Having the Nafion film cast directly on top of P-90/GOx instead of using a compartment separator (**Figure S13C**) improved the stability of the cell; the EFC maintains in average 45% of its OCV and 30% of its PD after 30 days. This direct encapsulation strategy aids in enzyme stabilization when intended for long term use.

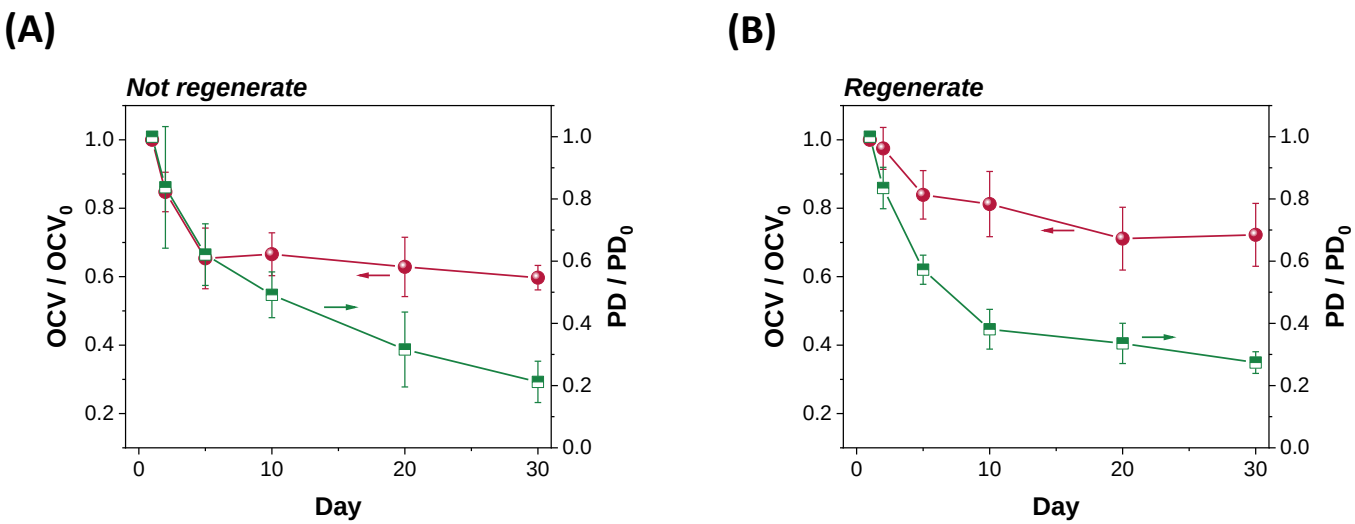

Figure S14. Long term stability of the membrane-free EFC. Relative voltage (OCV/OCV_0) measured at open circuit conditions and relative power (PD/DP_0) of the EFC fueled by 1 mM of glucose in PBS. **(A)** The enzyme is adsorbed on the anode at day 0 and kept as is until day 30, **(B)** the enzyme is replenished before each measurement.

When the enzyme is not replenished (**Figure S14A**), the OCV drops to 53% of its original value after 30 days, while the EFC retains 20% of its initial MPD, mainly due to the denaturation of the enzyme. Upon continuous replenishing of the GOx on P-90 (**Figure S14B**), superior performance is attested with an OCV and PD retention of 70% and 30%, respectively.

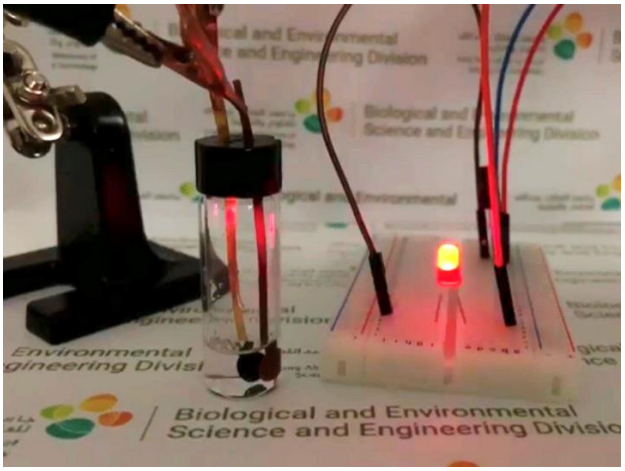

Figure S15. Digital photograph of a membrane-free EFC lighting an LED up. The device is fueled by 1 mM glucose in PBS.

References

1. Wang, B.; Li, B.; Deng, Q.; Dong, S., Amperometric Glucose Biosensor Based on Sol−Gel Organic−Inorganic Hybrid Material. *Anal. Chem* **1998,** *70* (15), 3170-3174.
2. Ozoemena, K. I.; Nyokong, T., Novel amperometric glucose biosensor based on an ether-linked cobalt(II) phthalocyanine–cobalt(II) tetraphenylporphyrin pentamer as a redox mediator. *Electrochim. Acta* **2006,** *51* (24), 5131-5136.
3. Ang, L. F.; Por, L. Y.; Yam, M. F., Development of an amperometric-based glucose biosensor to measure the glucose content of fruit. *PLoS One* **2015,** *10* (3), e0111859-e0111859.
4. Salimi, A.; Sharifi, E.; Noorbakhsh, A.; Soltanian, S., Immobilization of glucose oxidase on electrodeposited nickel oxide nanoparticles: Direct electron transfer and electrocatalytic activity. *Biosens. Bioelectron* **2007,** *22* (12), 3146-3153.
5. Zhang, S.; Wang, N.; Yu, H.; Niu, Y.; Sun, C., Covalent attachment of glucose oxidase to an Au electrode modified with gold nanoparticles for use as glucose biosensor. *Bioelectrochemistry* **2005,** *67* (1), 15-22.
6. Christwardana, M.; Kim, K. J.; Kwon, Y., Fabrication of Mediatorless/Membraneless Glucose/Oxygen Based Biofuel Cell using Biocatalysts Including Glucose Oxidase and Laccase Enzymes. *Sci. Rep* **2016,** *6*, 30128.
7. Christwardana, M.; Chung, Y.; Kwon, Y., Co-immobilization of glucose oxidase and catalase for enhancing the performance of a membraneless glucose biofuel cell operated under physiological conditions. *Nanoscale* **2017,** *9* (5), 1993-2002.
8. Liu, Y.; Wang, M.; Zhao, F.; Xu, Z.; Dong, S., The direct electron transfer of glucose oxidase and glucose biosensor based on carbon nanotubes/chitosan matrix. *Biosens. Bioelectron* **2005,** *21* (6), 984-988.
9. Zhao, M.; Gao, Y.; Sun, J.; Gao, F., Mediatorless Glucose Biosensor and Direct Electron Transfer Type Glucose/Air Biofuel Cell Enabled with Carbon Nanodots. *Anal. Chem* **2015,** *87* (5), 2615-2622.
10. Çetin, M. Z.; Camurlu, P., An amperometric glucose biosensor based on PEDOT nanofibers. *RSC Adv.* **2018,** *8* (35), 19724-19731.
11. Lineweaver, H.; Burk, D., The Determination of Enzyme Dissociation Constants. *J. Am. Chem. Soc.* **1934,** *56* (3), 658-666.
12. Kim, J. H.; Hong, S.-G.; Wee, Y.; Hu, S.; Kwon, Y.; Ha, S.; Kim, J., Enzyme precipitate coating of pyranose oxidase on carbon nanotubes and their electrochemical applications. *Biosens. Bioelectron* **2017,** *87*, 365-372.
13. Kwon, C. H.; Ko, Y.; Shin, D.; Kwon, M.; Park, J.; Bae, W. K.; Lee, S. W.; Cho, J., High-power hybrid biofuel cells using layer-by-layer assembled glucose oxidase-coated metallic cotton fibers. *Nat. Commun.* **2018,** *9* (1), 4479.
14. Bao, S.-J.; Li, C. M.; Zang, J.-F.; Cui, X.-Q.; Qiao, Y.; Guo, J., New Nanostructured TiO2 for Direct Electrochemistry and Glucose Sensor Applications. *Adv. Funct. Mater.* **2008,** *18* (4), 591-599.
15. Hu, Z.; Kang, Z.; Yu, C.; Wang, B.; Jiao, S.; Peng, R., Direct electron transfer of glucose oxidase in carbon paper for biofuel cells and biosensors. *Int. J. Electrochem. Sci* **2017,** *12*, 7103-7120.
16. Campbell, A. S.; Jeong, Y. J.; Geier, S. M.; Koepsel, R. R.; Russell, A. J.; Islam, M. F., Membrane/Mediator-Free Rechargeable Enzymatic Biofuel Cell Utilizing Graphene/Single-Wall Carbon Nanotube Cogel Electrodes. *ACS Appl. Mater. Interfaces* **2015,** *7* (7), 4056-4065.
17. Christwardana, M.; Kim, D.-H.; Chung, Y.; Kwon, Y., A hybrid biocatalyst consisting of silver nanoparticle and naphthalenethiol self-assembled monolayer prepared for anchoring glucose oxidase and its use for an enzymatic biofuel cell. *Appl. Surf. Sci.* **2018,** *429*, 180-186.

18. Kang, Z.; Jiao, K.; Yu, C.; Dong, J.; Peng, R.; Hu, Z.; Jiao, S., Direct electrochemistry and bioelectrocatalysis of glucose oxidase in CS/CNC film and its application in glucose biosensing and biofuel cells. *RSC Adv.* **2017,** *7* (8), 4572-4579.
19. Liu, Y.; Zhang, J.; Cheng, Y.; Jiang, S. P., Effect of Carbon Nanotubes on Direct Electron Transfer and Electrocatalytic Activity of Immobilized Glucose Oxidase. *ACS Omega* **2018,** *3* (1), 667-676.
20. Coman, V.; Vaz-Domínguez, C.; Ludwig, R.; Harreither, W.; Haltrich, D.; De Lacey, A. L.; Ruzgas, T.; Gorton, L.; Shleev, S., A membrane-, mediator-, cofactor-less glucose/oxygen biofuel cell. *Phys. Chem. Chem. Phys.* **2008,** *10* (40), 6093-6096.
21. Coman, V.; Ludwig, R.; Harreither, W.; Haltrich, D.; Gorton, L.; Ruzgas, T.; Shleev, S., A Direct Electron Transfer-Based Glucose/Oxygen Biofuel Cell Operating in Human Serum. *Fuel Cells* **2010,** *10* (1), 9-16.
22. Pan, C.; Fang, Y.; Wu, H.; Ahmad, M.; Luo, Z.; Li, Q.; Xie, J.; Yan, X.; Wu, L.; Wang, Z. L.; Zhu, J., Generating Electricity from Biofluid with a Nanowire-Based Biofuel Cell for Self-Powered Nanodevices. *Adv. Mater.* **2010,** *22* (47), 5388-5392.
23. Zebda, A.; Gondran, C.; Le Goff, A.; Holzinger, M.; Cinquin, P.; Cosnier, S., Mediatorless high-power glucose biofuel cells based on compressed carbon nanotube-enzyme electrodes. *Nat. Commun.* **2011,** *2*, 370.
24. Wang, X.; Falk, M.; Ortiz, R.; Matsumura, H.; Bobacka, J.; Ludwig, R.; Bergelin, M.; Gorton, L.; Shleev, S., Mediatorless sugar/oxygen enzymatic fuel cells based on gold nanoparticle-modified electrodes. *Biosens. Bioelectron* **2012,** *31* (1), 219-225.
25. Falk, M.; Andoralov, V.; Blum, Z.; Sotres, J.; Suyatin, D. B.; Ruzgas, T.; Arnebrant, T.; Shleev, S., Biofuel cell as a power source for electronic contact lenses. *Biosens. Bioelectron* **2012,** *37* (1), 38-45.
26. Kang, Z.; Jiao, K.; Cheng, J.; Peng, R.; Jiao, S.; Hu, Z., A novel three-dimensional carbonized PANI1600@CNTs network for enhanced enzymatic biofuel cell. *Biosens. Bioelectron* **2018,** *101*, 60-65.
27. Hoshi, K.; Muramatsu, K.; Sumi, H.; Nishioka, Y., Graphene-coated carbon fiber cloth for flexible electrodes of glucose fuel cells. *Jpn. J. Appl. Phys* **2016,** *55* (2S), 02BE05.
28. Escalona-Villalpando, R. A.; Hasan, K.; Milton, R. D.; Moreno-Zuria, A.; Arriaga, L. G.; Minteer, S. D.; Ledesma-García, J., Performance comparison of different configurations of Glucose/O2 microfluidic biofuel cell stack. *J. Power Sources* **2019,** *414*, 150-157.
29. Zhang, Y.; Savva, A.; Wustoni, S.; Hama, A.; Maria, I. P.; Giovannitti, A.; McCulloch, I.; Inal, S., Visualizing the Solid–Liquid Interface of Conjugated Copolymer Films Using Fluorescent Liposomes. *ACS Appl. Bio Mater.* **2018,** *1* (5), 1348-1354.
30. Wang, J., Electrochemical Glucose Biosensors. *Chem. Rev.* **2008,** *108* (2), 814-825.
31. Milton Ross, D.; Minteer Shelley, D., Direct enzymatic bioelectrocatalysis: differentiating between myth and reality. *J. Royal Soc. Interface* **2017,** *14* (131), 20170253.
32. Giussani, E.; Fazzi, D.; Brambilla, L.; Caironi, M.; Castiglioni, C., Molecular Level Investigation of the Film Structure of a High Electron Mobility Copolymer via Vibrational Spectroscopy. *Macromolecules* **2013,** *46* (7), 2658-2670.
33. Navarrete, J. T. L.; Zerbi, G., Lattice dynamics and vibrational spectra of polythiophene. II. Effective coordinate theory, doping induced, and photoexcited spectra. *J. Chem. Phys.* **1991,** *94* (2), 965-970.
34. Kergoat, L.; Piro, B.; Simon, D. T.; Pham, M.-C.; Noël, V.; Berggren, M., Detection of Glutamate and Acetylcholine with Organic Electrochemical Transistors Based on Conducting Polymer/Platinum Nanoparticle Composites. *Adv. Mater.* **2014,** *26* (32), 5658-5664.
35. Pappa, A.-M.; Curto, V. F.; Braendlein, M.; Strakosas, X.; Donahue, M. J.; Fiocchi, M.; Malliaras, G. G.; Owens, R. M., Organic Transistor Arrays Integrated with Finger-Powered Microfluidics for Multianalyte Saliva Testing. *Adv. Healthcare Mater.* **2016,** *5* (17), 2295-2302.

36. Mao, S.; Wen, Z.; Huang, T.; Hou, Y.; Chen, J., High-performance bi-functional electrocatalysts of 3D crumpled graphene–cobalt oxide nanohybrids for oxygen reduction and evolution reactions. *Energy Environ. Sci* **2014,** *7* (2), 609-616.
37. Laviron, E., General expression of the linear potential sweep voltammogram in the case of diffusionless electrochemical systems. *J. electroanal. chem. interfacial electrochem.* **1979,** *101* (1), 19-28.
38. Choi, S.; Chae, J., An array of microliter-sized microbial fuel cells generating 100μW of power. *Sens. Actuator A-Phys.* **2012,** *177*, 10-15.
39. Ye, D.; Yang, Y.; Li, J.; Zhu, X.; Liao, Q.; Deng, B.; Chen, R., Performance of a microfluidic microbial fuel cell based on graphite electrodes. *Int. J. Hydrog. Energy* **2013,** *38* (35), 15710-15715.
40. Jeon, W.-Y.; Lee, J.-H.; Dashnyam, K.; Choi, Y.-B.; Kim, T.-H.; Lee, H.-H.; Kim, H.-W.; Kim, H.-H., Performance of a glucose-reactive enzyme-based biofuel cell system for biomedical applications. *Sci. Rep* **2019,** *9* (1), 10872.